Physica E 134 (2021) 114826

Contents lists available at ScienceDirect

Physica E: Low-dimensional Systems and Nanostructures

journal homepage: www.elsevier.com/locate/physe

Anisotropy of effective masses induced by strain in Janus MoSSe and WSSe monolayers

M. Farkous [a,b,*], M. El-Yadri [b], H. Erguig [a], L.M. Pérez [c], D. Laroze [c], Chuong V. Nguyen [d], Nguyen T.T. Binh [e], Nguyen N. Hieu [e], Huynh V. Phuc [f], M. Sadoqi [g], G. Long [g], E. Feddi [b,**]

[a] Laboratoire d'Ingènieries des Systémes Electriques et des Tèlècommunications, Ecole Nationale des Sciences Appliquèes de Kènitra (ENSAK), Morocco
[b] LaMCScI, Group of Optoelectronic of Semiconductors and Nanomaterials, ENSAM, Mohammed V University in Rabat, Rabat, Morocco
[c] Instituto de Alta Investigación, Universidad de Tarapacá, Casilla 7D, Arica, Chile
[d] Department of Materials Science & Engineering, Le Quy Don Technical University, Ha Noi, Viet Nam
[e] Institute of Research and Development, Duy Tan University, Da Nang, Viet Nam
[f] Division of Theoretical Physics, Dong Thap University, Cao Lanh, Viet Nam
[g] Department of Physics, St John's University, Jamaica, NY, 11439, USA

ARTICLE INFO

Keywords:
Effective masses
Strain engineering
DFT calculations

ABSTRACT

In this work, the influence of biaxial strain on electronic, optical, and effective masses characteristics of Janus MSSe (M = Mo, W) have been investigated through first-principles calculations as implemented in WIEN2k package. From the obtained results, we remark that MoSSe and WSSe monolayers exhibit, respectively, a direct and indirect bandgap transition at equilibrium. Our achieved results demonstrate that the biaxial strain fundamentally alters the electronic states of Janus MSSe monolayers, and mainly, a semiconductor-metal transition phase has been determined to occur at a biaxial strain ratio of 12%. Moreover, it has been revealed that both electrons and holes effective masses of MSSe monolayers can be tuned by biaxial strain. For the optical properties of Janus monolayers, the polarization direction of the incident light plays a vital role in defining the light absorption domain. The MSSe Janus monolayers are shown to have a wide range of absorption spectrum, including the visible light domain with perpendicular polarized light. Furthermore, our computations of the dielectric function indicate that the optical responses of Janus monolayers MoSSe and WSSe strongly depend on the applied strain ratio; particularly, for the high photon energy domain. Overall, the findings revealed that both Janus MoSSe and WSSe monolayers could be potential materials for applications in optoelectronics.

1. Introduction

Transition metal dichalcogenides (TMDs) are one of the most extensively studied materials family in two-dimensional (2D) nanomaterials, which has shown many promising applications in next-generation optoelectronic devices [1–4] due to their outstanding mechanical, optical, chemical, thermal, and electronic properties [5–10]. Recently, a novel type of 2D material of Janus structures has attracted scientists' attention based on their intrinsic properties. Synthesized Janus MoSSe monolayer in the 2H phase has been successfully achieved by chemical vapor deposition and thermal selenization methods using pure MoS_2 monolayers through completely replacing the top layer of S atoms by Se atoms [11,12]. Also, WSSe monolayer has been successfully synthesized by chemical vapor deposition (CVD) [13].

Janus TMDs materials have unique characteristics such as strong Rashba spin splitting, second harmonic generation responses, large piezoelectric effect, excellent catalytic performance, making them potential candidates for optoelectronics, photovoltaics, and nanogenerators applications [14–17]. Recent theoretical investigations have focused on Janus monochalcogenides and Janus TMDs materials [18–20]. The mirror symmetry breaking encountered in Janus TMDs structure, which has been experimentally confirmed by scanning transmission electron microscopy [14], leads to the emergence of new physicochemical properties compared to 2D TMDs materials [19,21].

* Corresponding author. Laboratoire d'Ingènieries des Systémes Electriques et des Tèlècommunications, Ecole Nationale des Sciences Appliquèes de Kènitra (ENSAK), Morocco.
** Corresponding author.
E-mail addresses: mohammedfarkous@gmail.com (M. Farkous), e.feddi@um5s.net.ma (E. Feddi).

https://doi.org/10.1016/j.physe.2021.114826
Received 28 October 2020; Received in revised form 2 April 2021; Accepted 17 May 2021
Available online 26 May 2021

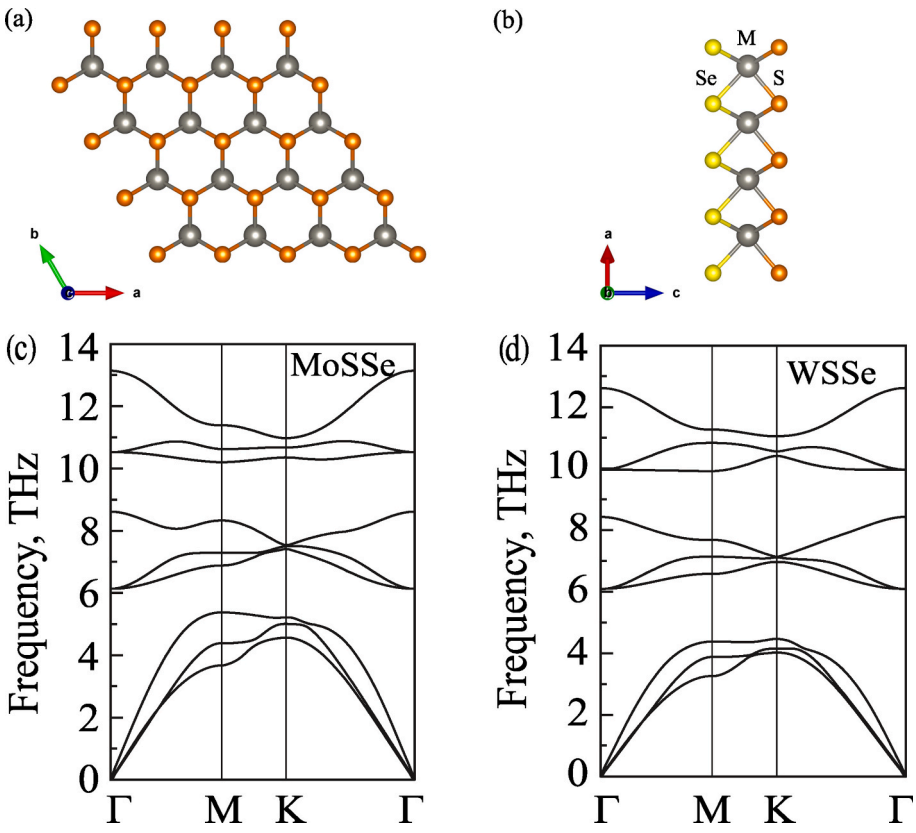

Fig. 1. (a) Top and (b) side views of the atomic structure of MSSe (M = Mo and *W*) monolayers. Phonon dispersion plots of Janus (c) MoSSe and (d) WSSe monolayers.

This paper proposes a theoretical investigation of the optoelectronic characteristics of MSSe Janus monolayers under the structural strain effect. The biaxial strain and the incoming photon energy range between 0 and 10 eV are considered to examine the main parameters of the above properties. The article is arranged as follows: Section 2 outlines the input parameters and the methods of calculations used to compute the opto-electronic properties of the considered materials. Section 3 presents a profound discussion of the obtained results, and in the last section, we outline some important points concerning the study.

2. Details of calculations

Calculations have been performed using the WIEN2k package based on the full-potential linearized augmented plane wave (FP-LAPW) method [22]. The Generalized Gradient Approximation based on the parametrization of Perdew, Burke, and Ernzerhof (GGA-PBE) was first employed to optimize the Janus MoSSe and WSSe monolayers structures [23]. For the fact that van der Waals (vdW) force is not accounted for in standard GGA functional, the atom-pairwise and atom-triple wise dispersion corrections (DFT-D3) suggested by Grimme [24,25] along with the Becke-Johnson (BJ) damping function [26] were used to treat the vdW interactions in the Janus structures. The effect of spin-orbit coupling (SOC) on the electronic properties of the Janus MSSe monolayers is essential. In all electronic properties calculations, PBE functional with SOC (PBE + SOC) was self-consistently employed. After total energy convergence tests, the Brillouin zone was sampled using a Monkhorst-Pack mesh of 21 × 21 × 1, making harmonic expansion up to $l_{max} = 10$ in each of the atomic spheres. The energy cut-off parameter $R_{mt}{}^{*}K_{max}$ was set to 9.0, where R_{mt} is the smallest atomic sphere radius in the unit cell, and K_{max} is the maximum value of the reciprocal lattice vector in the plane wave expansion. The Muffin-tin (MT) radii for Mo, W, S, and Se atoms were set to 2.38, 2.44, 2.05, and 2.32 a.u., respectively. In all calculations, the total energy and charge in self-consistency were iterated until accuracy up to 10^{-5} Ry and $10^{-4}e$, respectively. The full relaxations of the internal atomic position parameters are performed until all forces were inferior to 1 mRy/Bohr. To prevent periodic interaction, a vacuum layer thickness of 25 Å is added. The phonon spectrum and harmonic interatomic force constants were investigated through the density functional perturbation theory (DFPT) scheme via Phonopy code [27,28] with a supercell of 4 × 4 × 1. In order to ensure the convergence of the density of states (DOS) and the optical absorption spectrum, we have adopted to use a Monkhorst-Pack mesh of 100 × 100 × 1.

To quantitatively estimate the effects of the biaxial strain, we define the biaxial strain ϵ_b via the lattice constants of the monolayer before strain l_0 and after strain l as: $\epsilon_b = (l - l_0)/l_0$. Negative and positive values of the refer to the monolayer under compressive and tensile strains, respectively. We would like to underline the fact that the strains applied are the ones which are physically possible to apply in experiments. The strain engineering has been successfully applied experimentally to graphene in different studies [29–31]. Experimentally, in-plane strain can be introduced in mono- and multi-layers in a number of ways [29,30], such as depositing them onto flexible substrates, by subjecting them to external load, by pseudomorphic growth and nanoindentation of the mono/bi layers. The maximum biaxial tensile strain in the monolayer graphene has been observed experimentally up to 25% [29], before breaking the C–C bond in the sheet. Other authors have reported in-plane strain up to 6–11% for ultrathin MoS2 [31] using the nano-indentation method.

Table 1
Optimized lattice constants a, atomic bond lengths ($d_{M\text{-}S}$, $d_{M\text{-}Se}$, and $d_{S\text{-}Se}$), and bond angles $\left(S-\widehat{M}-S, S-\widehat{M}-Se, \text{and } Se-\widehat{M}-Se\right)$ of Janus MSSe (M = Mo and W) monolayers at equilibrium. Note that all lengths are in Å, and angles are in degree.

	a	$d_{M\text{-}S}$	$d_{M\text{-}Se}$	$d_{S\text{-}Se}$	$S-\widehat{M}-S$	$S-\widehat{M}-Se$	$Se-\widehat{M}-Se$
MoSSe	3.221	2.41	2.53	3.25	83.77	82.22	79.11
WSSe	3.226	2.41	2.53	3.27	83.49	84.53	78.93

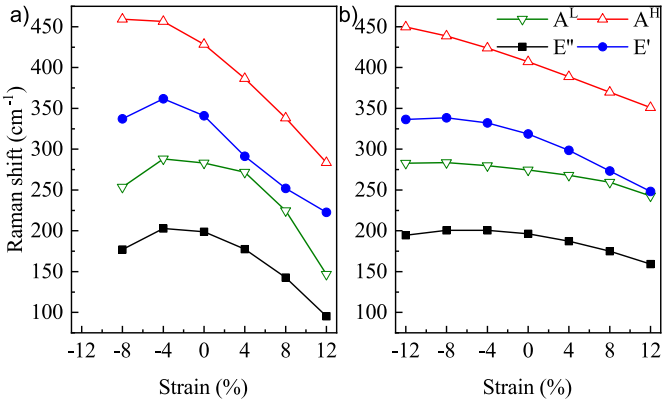

Fig. 2. Raman shift versus strain of Janus (a) MoSSe and (b) WSSe monolayers.

3. Results and discussions

3.1. Electronic properties

The Janus structure of MoSSe and WSSe monolayers can be built, respectively, from MoS_2 and WS_2 monolayers by substituting one of the S layers by Se layer, as can be shown in Fig. 1(a) and (b). In comparison with MS_2 (M = Mo or W) monolayers, the MSSe structure contains a reflection symmetry with respect to the central metal M atoms. Our calculations indicated that, at equilibrium, the optimized lattice constants a of the Janus monolayers MoSSe and WSSe are 3.221 Å and 3.226 Å, respectively. The basic structural parameters of Janus MoSSe and WSSe monolayers at the equilibrium state are summarized in Table 1.

To examine the dynamical stability of Janus MSSe monolayer under bi-axial strain, we calculate the phonon spectra, as shown in Fig. 1(c) and (d), where we can see that there are nine branches in the phonon spectrum of Janus MSSe monolayers. Such spectrm includes three acoustic and six optical branches, where the vibration representation of the optical modes is described as $\Gamma = 2E' + 2E'' + A^L + A^H$ [32]. The frequencies of the doubly degenerate in-plane optical modes for unstrained MoSSe, E'' and E', are 199 and 341 cm^{-1}, respectively, while those of unstrained WSSe, are 196 and 319 cm^{-1}, respectively. Besides those two optical modes, two others singly degenerate out-of-plane (A) optical modes are split as low-frequency A^L and high frequency A^H modes, which are 283 and 428 cm^{-1}, respectively, for unstrained MoSSe, and 275 and 407 cm^{-1}, respectively, for unstrained WSSe. There are no soft phonon modes (negative frequency) in both Janus MoSSe and WSSe monolayers, which means that both monolayers are dynamically stable. Our obtained phonon spectrum results (Figs. 1 and 2) are consistent with previous calculations [12,33].

Table 2
Calculated energy gaps using PBE E_{gap}^{nSOC} (eV) and PBE + SOC E_{gap}^{SOC} (eV), with their difference Δ (eV). The spin-orbit splitting values at K point around the Fermi level in the valence bands K_v (meV) and in the conduction bands K_c (meV). The effective masses for electrons (m_e^*/m_0) and holes (m_h^*/m_0), where m_0 is the free electron mass.

	E_{gap}^{nSOC}	E_{gap}^{SOC}	Δ	K_v	K_c	m_e^*/m_0	m_h^*/m_0	VBM/CBM
MoSSe	1.66	1.57	0.09	166	12	0.521	0.62	K/K
WSSe	1.77	1.42	0.35	436	38	0.495	0.39	K/Γ-K

Our Density Functional Theory (DFT) calculations demonstrate that Janus MoSSe is a direct bandgap semiconductor, where both conduction band minimum (CBM) and valence band maximum (VBM) are located at the high symmetry point K. On the other hand, Janus WSSe is an indirect bandgap semiconductor, where the CBM is located at the middle of K-Γ valleys and the VBM is located at the K-valley. At the equilibrium state, the energy gap value is founded to be equal to 1.66 eV for MoSSe Janus monolayer and 1.77 eV for WSSe. It is well-known that the SOC effect has a crucial impact on the electronic properties of TMDs materials with heavy metal atoms. Thus, after including the SOC effect in the calculations, the achieved band structures depicted in Fig. 3 shows a significant difference in the bandgap energies of the considered Janus monolayers compared to the case without SOC. The MoSSe band gap energy is reduced by 5.42% and for WSSe by 19.77%. Also, the spin-orbit energy value Δ of Janus WSSe monolayer (0.35 eV) is quite more significant than that of Janus MoSSe monolayer (0.09 eV) as listed in Table 2. Focusing on the partial density of states (PDOS) of Janus MSSe monolayers, and while the conduction bands are mainly dominant by M-d orbitals, the valence bands are equally composed of M-d, Se-p, and S-p orbitals. In the presence of biaxial strain, Janus monolayer structure is significantly changed. In this work, a wide biaxial strain range from −12% to 12% was applied to Janus monolayers. Our obtained results demonstrated that the bond angle $Se-\widehat{M}-S$ decreases linearly as the

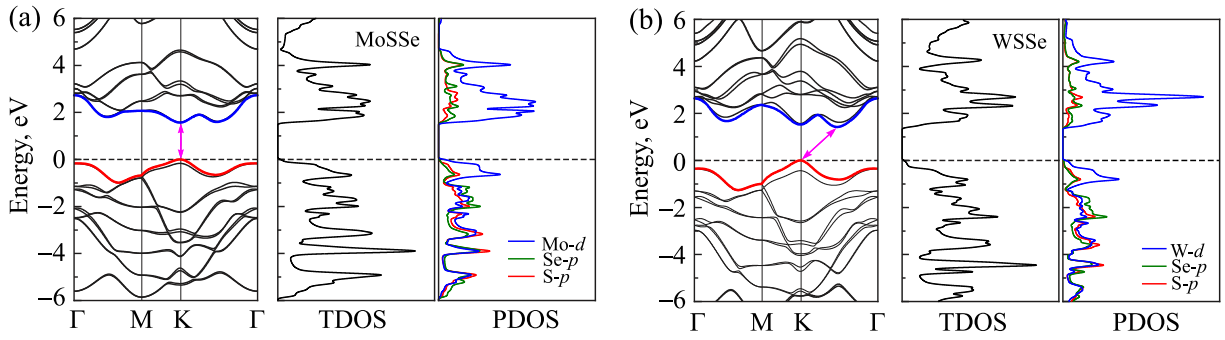

Fig. 3. Band structure and density of states at equilibrium of Janus (a) MoSSe and (b) WSSe monolayers.

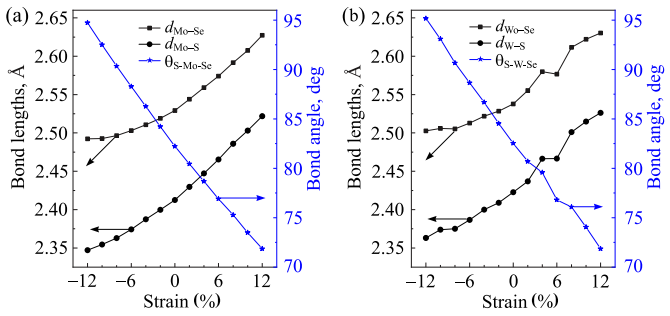

Fig. 4. Calculated interatomic distances (d_{M-S}andd_{M-Se}) and bond angles $Se-\widehat{M}-S$ versus strain of Janus (a) MoSSe and (b) WSSe monolayers.

strain increases. Dependence of the bond lengths and bond angles on the biaxial strain are depicted in Fig. 4.

Let us now discuss the mechanism of the biaxial strain ϵ_b and its action on the basic electronic properties of the two MSSe Janus monolayers based on the achieved results with PBE + SOC approach. For a best description of this step, ϵ_b makes use of the optimized lattice constants before and after applied strain noted l_0 and l, respectively, following the formula $\epsilon_b = (l - l_0)/l_0$.

The effect of biaxial strain on electronic properties is fascinating. The calculated band structures of strained Janus MSSe are shown in Fig. 5. As above-mentioned, Janus MoSSe monolayer is a direct gap semiconductor with both CBM and VBM locating at the K-point in the first Brillouin zone. However, the difference in energy between the highest energy of the valence band at the Γ-point and the VBM is quite small. This leads the expectation that we can change the characteristics of the monolayer bandgap by external conditions such as strain engineering or electric field. As shown in Fig. 5, we can see that in the presence of the biaxial strain ϵ_b, the band structure of Janus MoSSe monolayer is significantly changed. When the biaxial strained was introduced, Janus MoSSe monolayer becomes an indirect gap semiconductor. Also, the bandgap of Janus MoSSe decreases rapidly with increasing the biaxial strains, especially in the case of the tensile biaxial strain. The bandgap of Janus MoSSe monolayer decreases to zero at a considerable biaxial strain of 12%. It means that a semiconductor-metal phase transition occurs for the case of Janus MoSSe monolayer at the $\epsilon_b = 12\%$.

The application of biaxial strains alters both bond lengths and bond angles, as well as modulate the coupling strengths of the orbitals. Several theoretical works have reported that M-*d*, S-*p*, Se-*p* orbitals of the chalcogen atoms plays an important role to modulate the band gaps [34]. Moreover, and for more details on the bandgap behavior under biaxial strains, it is necessary to analyze the contributions of M-d_{z^2}, M-$d_{x^2-y^2} + d_{xy}$, Se-*p*, and S-*p* orbitals on the electronic properties, as presented in Fig. 7. From both Figs. 5 and 7, we can see that, the VBM at Γ and the CBM at K are both dominated by M-d_{z^2} (see $\epsilon_b = 8\%$), while a strong in-plane orbitals $d_{x^2-y^2} + d_{xy}$ characters are located in the VBM at K-point and CBM at the local minimum point of the lowest conduction band along the K to Γ direction.

As already shown in Fig. 4, the tensile strains on MSSe monolayers increase the bond lengths of d_{M-S} and d_{M-Se}, which in turn reduce the S-M-Se angle, and therefore the coupling between M-d_{z^2},Se-*p*, and S-*p* orbitals becomes weaker, while the coupling between the in-plane orbitals $d_{x^2-y^2} + d_{xy}$, Se-*p*, and S-*p* orbitals becomes stronger.

These modifications of couplings lead to the appearance of two effects. Firstly, M-d_{z^2} shift to lower energy in conduction band at the K-point and to higher energy in the valence band at the Γ-point, which reduces the gap between valence and conduction bands at the Γ-point and K-point, respectively, due to the weak orbit coupling between the M-d_{z^2}, Se-*p*, and S-*p* orbitals. The second effect is the expansion of the gap between the valence and conduction bands at the K-point and the middle of K-Γ-point, respectively, due to the strong orbit coupling between the $d_{x^2-y^2} + d_{xy}$, Se-*p*, and S-*p* orbitals. By applying tensile strain of 2%, Mo-d_{z^2} orbital cross the Mo-$d_{x^2-y^2} + d_{xy}$ orbital in the valence band; thus, MoSSe monolayer becomes an indirect gap semiconductor.

In contrast to tensile strains, compressive strains reduce the bond lengths d_{M-S} and d_{M-Se}, which leads to an increase in the S-M-Se bond angle. Increases of the S-M-Se angle strengthens the coupling between M-d_{z^2}, Se-*p*, and S-*p* orbitals and weakens coupling between the in-plane orbitals $d_{x^2-y^2} + d_{xy}$, Se-*p*, and S-*p*. Hence, these modifications of couplings expanse the gap between valence band at the Γ-point and conduction band at the K-point (M-d_{z^2} orbitals shift to the higher energy in the CB at K-point) while reduce the gap between the CB at the middle of

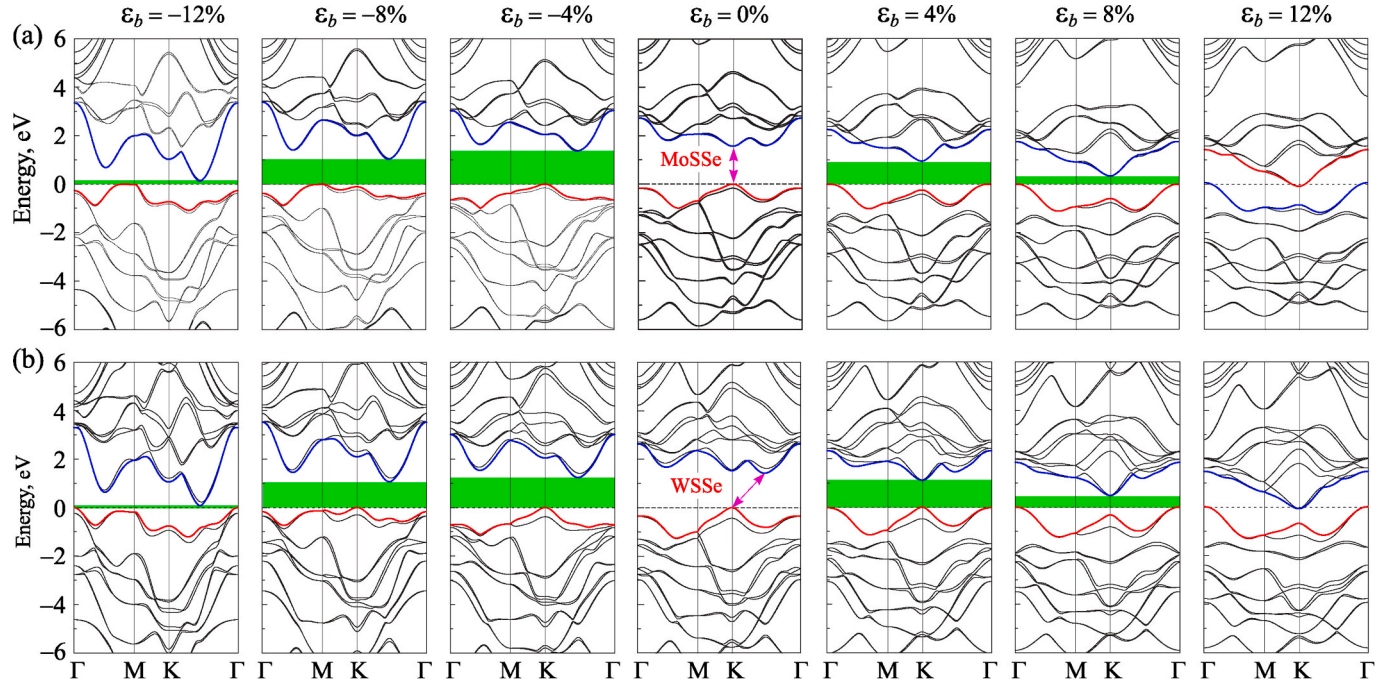

Fig. 5. Band structures of Janus (a) MoSSe (b) and WSSe monolayers under different levels of biaxial strains ϵ_b.

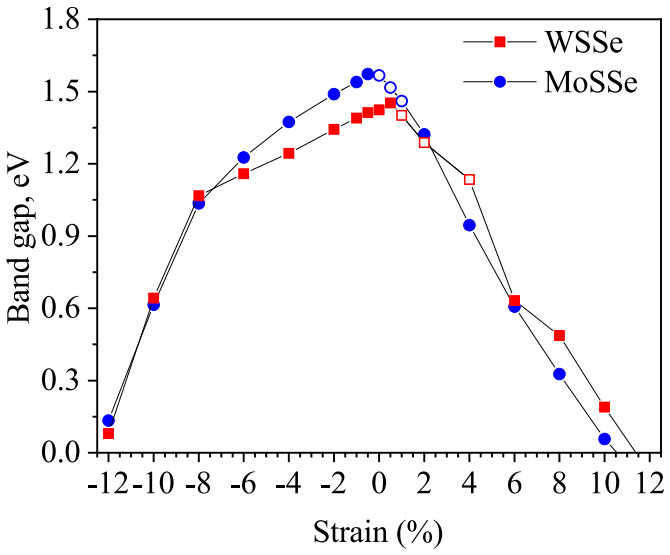

Fig. 6. The bandgap of Janus monolayers WSSe and MoSSe obtained with PBE + SOC as a function of strain. Note that open circles and squares represent direct bandgap transitions of MoSSe and WSSe monolayers, respectively.

K-Γ point. In the conduction band, Mo-$d_{x^2-y^2} + d_{xy}$ orbital cross Mo-d_{z^2} orbital by an applied compressive strain of 0.5%, hence a direct-to-indirect band gap transition occur for MoSSe monolayer. These bandgaps behavior as function of strains obtained for Janus MSSe is similar to the one found for TMDs monolayers (such MoS_2 and WS_2) under various strains [35,36].

Dependence of MSSe monolayer bandgap on the biaxial strain is depicted in Fig. 6. The biaxial strain not only leads to the direct-indirect gap transition in Janus MSSe monolayers, but also causes the semiconductor-metal phase transition to occur. Similar to Janus MoSSe monolayer, the band structure of Janus WSSe depends strongly on the ϵ_b, as illustrated in Fig. 5(b); even if the bandgap of Janus WSSe decreases rapidly in the presence of biaxial strain ϵ_b. In the range from −12% to 12%, Janus WSSe monolayer is an indirect bandgap semiconductor; whereas, in the interval from 1% to 4%, Janus WSSe monolayer is a direct semiconductor.

In addition to the band gaps, the effective masses $m^* = \hbar^2 / \frac{\partial^2 E}{\partial k^2}$ are estimated by fitting the bands to a parabola for a small range of wave vector along the valence and the conduction bands, where E is the energy, k is the wave vector and $\hbar$ is the reduced Planck constant. The electrons and holes effective masses at high-symmetry points are displayed in Fig. 8 and Fig. 9. As we know, the carrier effective masses not only can confirm the isotropic character of MSSe monolayers, but also strongly influence the carrier mobility, the smaller value of effective mass indicates a higher mobility and faster transfer rate of charge carriers [37,38]. At equilibrium, our results show that the electrons m_e^* and holes m_h^* effective masses of MoSSe (WSSe) are $0.521m_0$ ($0.495m_0$) and $0.62m_0$ ($0.39m_0$), respectively. These values also well agree with recent theoretical results [39,40].

The calculated effective masses for conduction and valence bands under both tensile and compressive biaxial strains of MSSe monolayers are illustrated in Fig. 9. The effective masses of Janus MSSe monolayers can be tuned via strains engineering. As presented in Fig. 9, the electron effective masses are found to be depended linearly on the strains. The electrons and holes effective masses increases (decreases slightly) when the biaxial compressive (tensile) strains increases at the K-valley. In the valence band, the Γ-valley effective masses decreases rapidly with increasing tensile strain, while the K-Γ-valleys masses stay fairly constant (see Fig. 9 (a) and (c)). Fig. 8 shows the calculated results of the effective masses at CBM and VBM under biaxial strains. The effective masses of holes encounters a significant fluctuation as the strains increases. These fluctuations are caused by the direct to indirect bandgaps transitions under biaxial strains (VBM changing from K-point to Γ-point). The strong electronic properties dependence on the applied strain in Janus MSSe monolayers is similar to the case of TMDs monolayers [41,42].

3.2. Optical properties

The optical properties usually are deemed as a critical for determining the potential applications of these materials in the electronic detectors and optoelectronic devices. In the present work, the optical properties of Janus MSSe (M = *Mo*, *W*) monolayers have been determined under both compressive and tensile biaxial strains for incoming photon energy range from 0 to 10 eV. We focus on the effect of biaxial

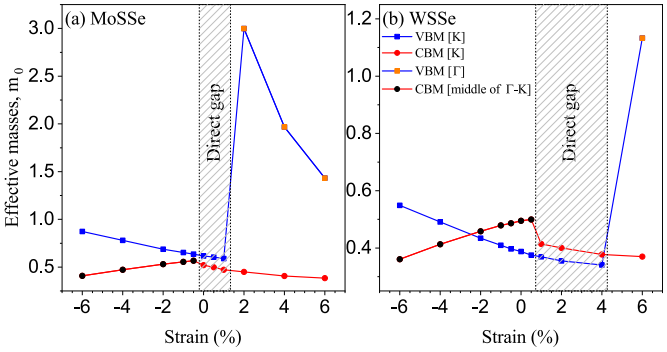

Fig. 8. The carrier effective masses with SOC for CBM and VBM of the Janus (a) MoSSe and (b) WSSe monolayers as a function of biaxial strains.

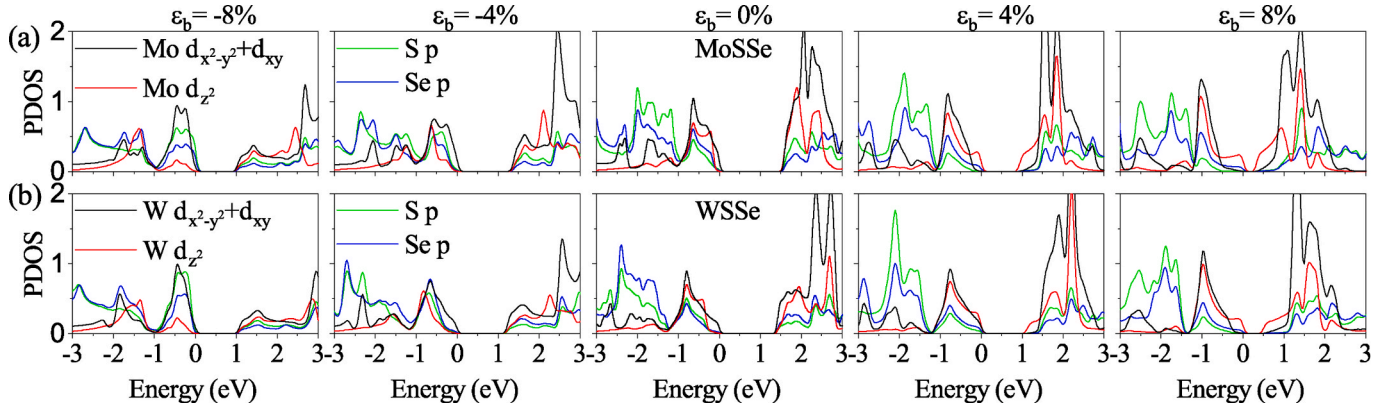

Fig. 7. Partial densities of states calculated for Janus (a) MoSSe and (b) WSSe monolayers under biaxial strains ϵ_b.

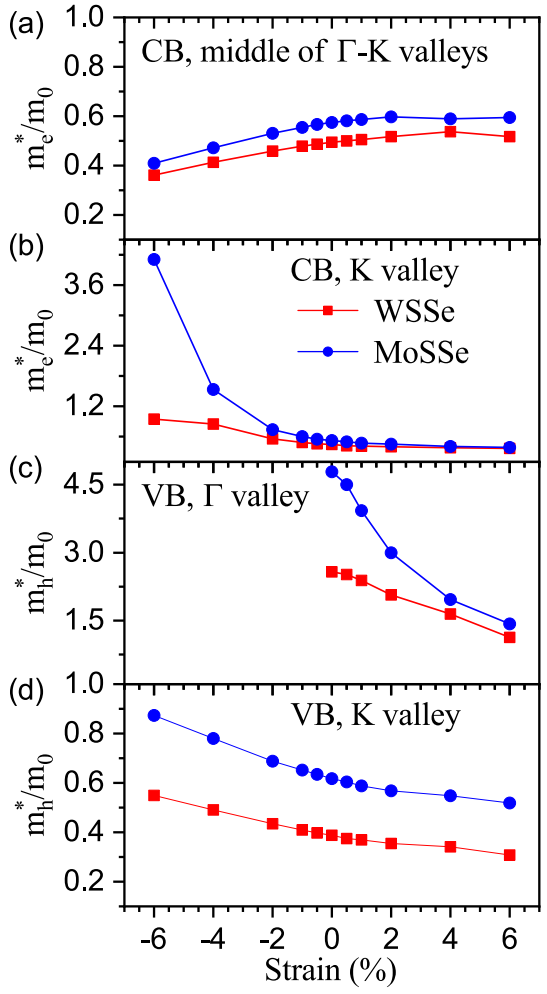

Fig. 9. Calculated effective masses of MoSSe and WSSe with SOC for the conduction band at (a) middle of Γ-K-valleys and (b) K-valley, as well as for the valence band at (c) Γ-valley and (d) K-valley under biaxial strains.

strain on the dielectric function $\epsilon(\omega)$ and absorption coefficient $\alpha(\omega)$ of Janus MSSe monolayers. The dielectric function can be defined via the real $\epsilon_1(\omega)$ and imaginary $\epsilon_2(\omega)$ parts as:

$$\epsilon(\omega) = \epsilon_1(\omega) + i\epsilon_2(\omega), \tag{1}$$

where ω is the angular frequency of the incident photon. The imaginary part $\epsilon_2(\omega)$ is calculated first by summing the transitions between filled-unfilled states and the real part of the dielectric function can be obtained then via the Kramer-Kronig relation. The imaginary part $\epsilon_2(\omega)$ is given by [?]:

$$\epsilon_2^{ij}(\omega) = \frac{4\pi^2 e^2}{Vm^2\omega^2}\sum_{knn'\sigma}\langle kn\sigma|p_i|kn'\sigma\rangle\langle kn'\sigma|p_j|kn\sigma\rangle \times f_{kn}(1-f_{kn'})\delta(E_{kn'}-E_{kn}-\hbar\omega), \tag{2}$$

where V is the volume of the unit cell, e and m are the charge and mass of the electron, respectively, and p is the momentum operator.

The calculated parts of the dielectric function of Janus MSSe monolayers are displayed in Fig. 10. Both perpendicular ($\perp$) and parallel ($\parallel$) polarized lights are individually considered in our calculations. Focusing on the imaginary part $\epsilon_2(\omega)$, our calculations demonstrated that while the first optical peaks in the case of perpendicular polarization $\epsilon_2^{\perp}(\omega)$ are located in the visible light region, the first optical peaks in the case of parallel polarization $\epsilon_2^{\parallel}(\omega)$ are shifted to higher photon energy domain and are located in ultraviolet region. These optical peaks directly correlate to the absorption range of Janus monolayers. In the case of parallel polarized light, the $\epsilon_2^{\parallel}(\omega)$ does not respond to the broad energy range of the incoming light from 0 to 2 eV for both Janus MoSSe and WSSe monolayers.

The absorption coefficient $\alpha(\omega)$ can be defined via the parts of the dielectric function as follows [43]:

$$\alpha(\omega) = \frac{\sqrt{2}\omega}{c}\left[\sqrt{\epsilon_1^2(\omega)+\epsilon_2^2(\omega)} - \epsilon_1(\omega)\right]^{1/2}. \tag{3}$$

The Influence of biaxial strain ϵ_b on $\alpha(\omega)$ of Janus MSSe monolayers is depicted in Fig. 11. We can see that Janus MSSe monolayer absorb visible light well in cases of parallel polarized light. However, in the case of photon energy range from 0 to 10 eV, the maximum value of $\alpha^{\perp}(\omega)$ is smaller than the one of $\alpha^{\parallel}(\omega)$. Effect of biaxial strain ϵ_b on $\alpha(\omega)$ is more evident in the large photon energy domain. The compressive strain increases the absorption coefficient of Janus MSSe monolayers, while the absorption coefficient is slightly reduced in the case of tensile strain.

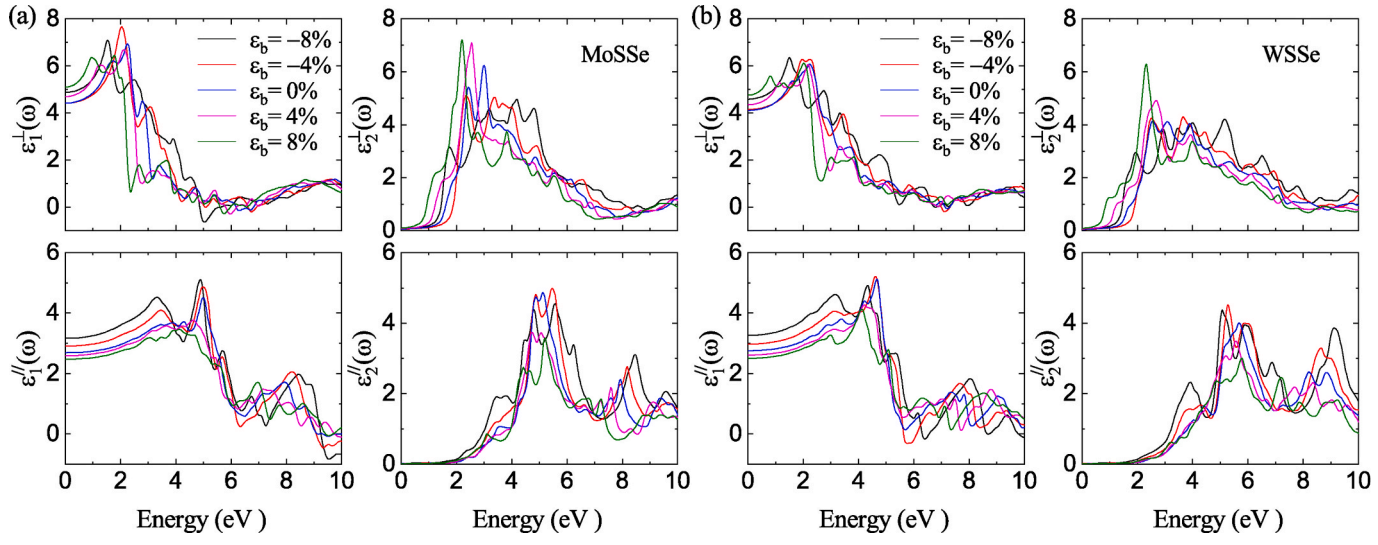

Fig. 10. Calculated real $\epsilon_1(\omega)$ and imaginary $\epsilon_2(\omega)$ parts of the dielectric function with PBE + SOC method of Janus (a) MoSSe and (b) WSSe under biaxial strains.

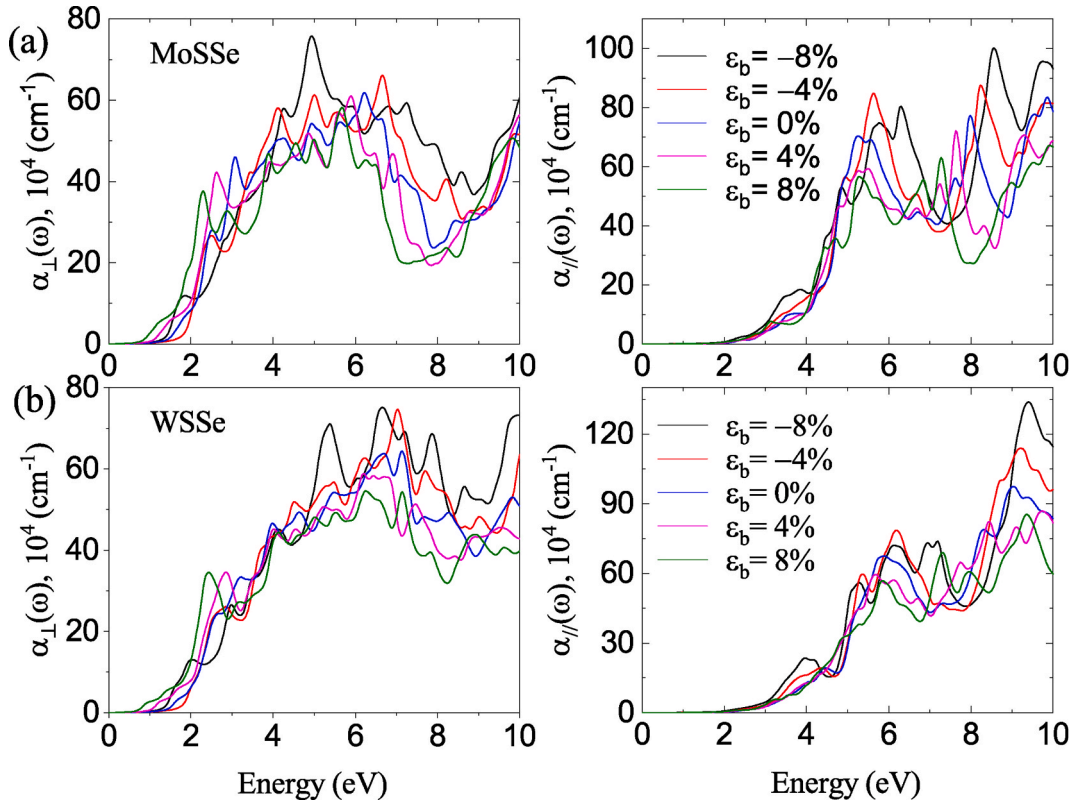

Fig. 11. Absorption coefficient $\alpha(\omega)$ of Janus MoSSe (a) and WSSe (b) monolayers under biaxial strains.

4. Conclusions

In summary, we have systematically studied the influence of biaxial strain on electronic, effective masses and optical properties of Janus MSSe (M = Mo, W) monolayers using first-principles calculations. Our findings revealed that, at the equilibrium state, Janus monolayers could exhibit a direct-indirect bandgap transition and a semiconductor-metal phase transition has been found at a specific strain ratio. Moreover, we have found that the electrons and holes effective masses can be significantly tuned by biaxial strain. Both Janus MoSSe and WSSe monolayers can powerfully absorb the visible light in the case of incoming perpendicular polarized light, and the absorption coefficient of Janus monolayer depends strongly on the biaxial strain, especially in the high photon energy range. All these results suggest that these Janus monolayers can be used for optoelectronic devices applications.

Declaration of competing interest

There are no conflicts to declare.

Acknowledgements

L. M. Pérez and D. Laroze acknowledge partial financial support from FONDECYT 1180905. D. Laroze acknowledges partial financial support from Centers of excellence with BASAL/CONICYT financing, Grant AFB180001, CEDENNA. G. Long would like to thank St John's University startup grant and Seed grant and Summer Research Support. E. Feddi and G. Long would like to thank CFN for providing facilities access. This research used resources of the Center for Functional Nanomaterials, which is a U.S. DOE Office of Science Facility, at Brookhaven National Laboratory under Contract No. DE-SC0012704.

References

[1] B. Radisavljevic, A. Radenovic, J. Brivio, V. Giacometti, A. Kis, Nat. Nanotechnol. 6 (2011) 147–150.
[2] O. Lopez-Sanchez, D. Lembke, M. Kayci, A. Radenovic, A. Kis, Nat. Nanotechnol. 8 (2013) 497–501.
[3] D. Jariwala, V.K. Sangwan, L.J. Lauhon, T.J. Marks, M.C. Hersam, ACS Nano 8 (2014) 1102–1120.
[4] P. Rivera, J.R. Schaibley, A.M. Jones, J.S. Ross, S. Wu, G. Aivazian, P. Klement, K. Seyler, G. Clark, N.J. Ghimire, et al., Nat. Commun. 6 (2015) 1–6.
[5] A. Castellanos-Gomez, M. Poot, G.A. Steele, H.S. Van der Zant, N. Agraït, G. Rubio-Bollinger, Nanoscale Research Letters 7 (2012) 233.
[6] K.F. Mak, K. He, J. Shan, T.F. Heinz, Nat. Nanotechnol. 7 (2012) 494–498.
[7] Q.H. Wang, K. Kalantar-Zadeh, A. Kis, J.N. Coleman, M.S. Strano, Nat. Nanotechnol. 7 (2012) 699–712.
[8] J.S. Ross, P. Klement, A.M. Jones, N.J. Ghimire, J. Yan, D. Mandrus, T. Taniguchi, K. Watanabe, K. Kitamura, W. Yao, et al., Nat. Nanotechnol. 9 (2014) 268–272.
[9] S. Manzeli, D. Ovchinnikov, D. Pasquier, O.V. Yazyev, A. Kis, Nature Reviews Materials 2 (2017) 17033.
[10] M. Farkous, M. Bikerouin, H.T. Phung, M. El-Yadri, E. Feddi, F. Dujardin, C. Duque, D. Muoi, H.V. Phuc, C.V. Nguyen, et al., Mater. Res. Express 6 (2019), 065060.
[11] J. Zhang, S. Jia, I. Kholmanov, L. Dong, D. Er, W. Chen, H. Guo, Z. Jin, V.B. Shenoy, L. Shi, et al., ACS Nano 11 (2017) 8192–8198.
[12] A.-Y. Lu, H. Zhu, J. Xiao, C.-P. Chuu, Y. Han, M.-H. Chiu, C.-C. Cheng, C.-W. Yang, K.-H. Wei, Y. Yang, et al., Nat. Nanotechnol. 12 (2017) 744–749.
[13] X. Duan, C. Wang, Z. Fan, G. Hao, L. Kou, U. Halim, H. Li, X. Wu, Y. Wang, J. Jiang, et al., Nano Lett. 16 (2016) 264–269.
[14] D. Er, H. Ye, N.C. Frey, H. Kumar, J. Lou, V.B. Shenoy, Nano Lett. 18 (2018) 3943–3949.
[15] C. Xia, W. Xiong, J. Du, T. Wang, Y. Peng, J. Li, Phys. Rev. B 98 (2018) 165424.
[16] R. Li, Y. Cheng, W. Huang, Small 14 (2018) 1802091.
[17] H. Cai, Y. Guo, H. Gao, W. Guo, Nanomater. Energy 56 (2019) 33–39.
[18] A. Huang, W. Shi, Z. Wang, J. Phys. Chem. C 123 (2019) 11388–11396.
[19] L. Dong, J. Lou, V.B. Shenoy, ACS Nano 11 (2017) 8242–8248.
[20] H. Din, M. Idrees, A. Albar, M. Shafiq, I. Ahmad, C.V. Nguyen, B. Amin, Phys. Rev. B 100 (2019) 165425.
[21] L. Cao, Y.S. Ang, Q. Wu, L. Ang, Appl. Phys. Lett. 115 (2019) 241601.
[22] P. Blaha, K. Schwarz, G.K. Madsen, D. Kvasnicka, J. Luitz, R. Laskowski, F. Tran, L. Marks, Vienna University of Technology, Austria, 2018.
[23] J.P. Perdew, A. Ruzsinszky, G.I. Csonka, O.A. Vydrov, G.E. Scuseria, L. A. Constantin, X. Zhou, K. Burke, Phys. Rev. Lett. 100 (2008) 136406.
[24] S. Grimme, J. Antony, S. Ehrlich, H. Krieg, J. Chem. Phys. 132 (2010) 154104.
[25] S. Grimme, S. Ehrlich, L. Goerigk, J. Comput. Chem. 32 (2011) 1456–1465.
[26] E.R. Johnson, A.D. Becke, J. Chem. Phys. 124 (2006) 174104.

[27] X. Gonze, C. Lee, Phys. Rev. B 55 (1997) 10355.
[28] A. Togo, I. Tanaka, Scripta Mater. 108 (2015) 1–5.
[29] C. Lee, X. Wei, J.W. Kysar, J. Hone, Science 321 (2008) 385–388.
[30] M. Huang, H. Yan, T.F. Heinz, J. Hone, Nano Lett. 10 (2010) 4074–4079.
[31] S. Bertolazzi, J. Brivio, A. Kis, ACS Nano 5 (2011) 9703–9709.
[32] A. Kandemir, H. Sahin, Phys. Chem. Chem. Phys. 20 (2018) 17380–17386.
[33] H. Liu, Z. Huang, C. He, Y. Wu, L. Xue, C. Tang, X. Qi, J. Zhong, J. Appl. Phys. 125 (2019), 082516.
[34] C.-H. Chang, X. Fan, S.-H. Lin, J.-L. Kuo, Phys. Rev. B 88 (2013) 195420.
[35] M. Farkous, M. Bikerouin, D.V. Thuan, Y. Benhouria, M. El-Yadri, E. Feddi, H. Erguig, F. Dujardin, C.V. Nguyen, N.V. Hieu, et al., Phys. E Low-dimens. Syst. Nanostruct. 116 (2020) 113799.
[36] P. Johari, V.B. Shenoy, ACS Nano 6 (2012) 5449–5456.
[37] M. Zhou, X. Chen, M. Li, A. Du, J. Mater. Chem. C 5 (2017) 1247–1254.
[38] J. Zhang, P. Zhou, J. Liu, J. Yu, Phys. Chem. Chem. Phys. 16 (2014) 20382–20386.
[39] W.-J. Yin, B. Wen, G.-Z. Nie, X.-L. Wei, L.-M. Liu, J. Mater. Chem. C 6 (2018) 1693–1700.
[40] J. Wang, H. Shu, T. Zhao, P. Liang, N. Wang, D. Cao, X. Chen, Phys. Chem. Chem. Phys. 20 (2018) 18571–18578.
[41] H.J. Conley, B. Wang, J.I. Ziegler, R.F. Haglund Jr., S.T. Pantelides, K.I. Bolotin, Nano Lett. 13 (2013) 3626–3630.
[42] W. Wu, L. Wang, Y. Li, F. Zhang, L. Lin, S. Niu, D. Chenet, X. Zhang, Y. Hao, T. F. Heinz, et al., Nature 514 (2014) 470.
[43] D. Hoat, J. Rivas Silva, A. Méndez Blas, J. Ríos Rámirez, Rev. Mexic. Fisica 64 (2018) 94–100.